Nonlinear Analysis: Real World Applications 39 (2018) 120–141

Contents lists available at ScienceDirect

Nonlinear Analysis: Real World Applications

www.elsevier.com/locate/nonrwa

On a free boundary problem for biosorption in biofilms

B. D'Acunto, L. Frunzo*, M.R. Mattei

Department of Mathematics and Applications "Renato Caccioppoli", University of Naples Federico II, Complesso Monte Sant'Angelo, 80124 Naples, Italy

ARTICLE INFO

Article history:
Received 4 October 2016
Received in revised form 14 June 2017
Accepted 21 June 2017

Keywords:
Biosorption
Multispecies biofilms
Hyperbolic free boundary value problem
Method of characteristics

ABSTRACT

The work presents the qualitative analysis of the free boundary value problem related to the biosorption process in multispecies biofilms. In the framework of continuum biofilm modeling, the mathematical problem consists of a system of nonlinear hyperbolic partial differential equations for microbial species growth and spreading, a system of semilinear parabolic partial differential equations describing the substrate trends and a system of semilinear parabolic partial differential equations accounting for the diffusion, reaction and biosorption of different agents on the various biofilm constituents. Two systems of nonlinear hyperbolic partial differential equations have been considered as well for modeling the dynamics of the free and bounded sorption sites. The free boundary evolution is regulated by a nonlinear ordinary differential equation. Overall, this leads to a free boundary value problem essentially hyperbolic. The main result is the existence and uniqueness of the solutions to the stated free boundary value problem, which have been derived by converting the partial differential equations to Volterra integral equations and then using the fixed point theorem. Moreover, the work is completed with numerical simulations for a real case examining the growth of a heterotrophic–autotrophic biofilm devoted to wastewater treatment and acting as a sorbing material for heavy metal biosorption.

1. Introduction

Over the years, biofilms have been recognized as the most prevalent form of microbial life in various habitats with medical, industrial, and ecological relevance [1]. Biofilms are mainly constituted by bacterial cells of a single or multiple different species in proximity one to another, associated to a solid surface or phase inter-phase and embedded in a self-produced primarily polysaccharide matrix [2]. The interspecies interactions [3,4], the presence of a multitasking matrix [5] and the structure itself, provide to the biofilm several capabilities, such as increased tolerance against antimicrobial agents [6] and protozoan grazing [7],

* Corresponding author.
E-mail addresses: dacunto@unina.it (B. D'Acunto), luigi.frunzo@unina.it (L. Frunzo), mariarosaria.mattei@unina.it (M.R. Mattei).

http://dx.doi.org/10.1016/j.nonrwa.2017.06.010
1468-1218/

improved degradation of organic compounds, high sorption properties for a variety of recalcitrant or slow-degrading compounds, e.g. toxic metal ions and xenobiotics, which are mainly exploited in the field of bioremediation and wastewater treatment [8]. The use of biomass as sorbents for the removal and recovery of organic and inorganic substances in gaseous, soluble or insoluble forms is known as *biosorption* [9]. The term traditionally refers to the passive physico-chemical metabolism-independent process, involving a solid phase (biosorbent) and a liquid phase containing the dissolved or suspended species to be sorbed (sorbate) (e.g. metals, dyes, fluoride, pharmaceuticals, phenols) and resulting in an accumulation at the sorbate–sorbent interface [10]. This relatively new process has become during the last years one of the most promising and cost-effective alternative technologies for the removal and recovery of a wide range of organic and inorganic compounds from industrial effluents and natural waters as it is characterized by a low cost, high removal efficiency, reduced chemical use, reuse potential of biomaterials and nutrients, and possibility of metal recovery [11]. Various materials of biological origin can be used as biosorbents, including plant biomass, bacteria, fungi, and algae, etc. [12]. Dead biomass has been preferred in most of experimental studies due to the following advantages: absence of toxicity limitations; easy absorbance and recovery of biosorbed metals; easy regeneration and reuse of biomass; possibility of easy immobilization of dead cells; easier mathematical modeling of metal uptake [10]. However, additional benefits might result from the metabolic activities (respiration, nutrient uptake, EPS, metabolite release and oxido-reductive transformations) of living organisms which might alter the microenvironment around the cells and contribute to the overall removal process. Biofilms have drawn particular interest in this context due to the abundant binding site concentration in both microbial cell walls and extracellular polymeric substances and the natural absence of toxicity limitations. The binding mechanism of the sorbate onto the biomass surface can be performed by many mechanisms occurring under different operating and environmental conditions, including electrostatic interactions, covalent binding, ions exchange, microprecipitation, chelation and complexation [13]. Biosorption efficiency is affected by various environmental factors, such as pH, which rules metal mobility and speciation, temperature, with an optimal value ranging between 20 and 35 C, and the co-presence of multiple heavy metals. Besides the factors above mentioned, the amount of sorbent used significantly affects process efficiency and stability as a higher sorbent concentration increases the availability of active sites that can effectively bind metal ions [13]. Although the high number of experimental studies on biosorption developed during the last decays, several aspects still need to be clarified for the scale-up of the process at the industrial scale.

In this context, mathematical modeling appears as a support to gain essential information for the identification of the key factors affecting biosorption efficiency and stability [14]. Due to process similarities to adsorption, conventional equilibrium and kinetics models have been adapted to the needs of the mathematical description of biosorption and applied to a wide range of batch experimental situations (see [13,15,16] for a recent overview). For single-metal solutions, the most widely used isotherm models are the two-parameter models of Langmuir and Freundlich, which correlate the sorbed and solute sorbate concentration in the liquid phase at equilibrium for constant environmental parameters. These models were originally derived for non-biological systems and are based on assumptions that are quite simplistic for such complex systems. They are not able to reproduce the mechanisms of solute uptake, but they have been widely recognized as efficient tools to provide a suitable description of the experimental behavior. Kinetic models are usually aimed at describing the behavior of the sorption system on time [17] and have been commonly applied to study the contribution of the main rate controlling steps (i.e. bulk diffusion; film diffusion; intraparticle diffusion; chemical reaction) invariably involved in the sorption process [13]. They usually come in the form of generally highly simplified pseudo-first and second order kinetic equations. The most used kinetic model is the Weber–Morris intraparticle diffusion model which describes well the kinetics of biosorption for the first 10 min of the process [10]. Mathematical models for continuous biosorption systems have been developed as well: they usually refer to a flow-through fixed-bed bioreactor configuration and have been originally derived

for research on activated carbon sorption, ion exchange, or chromatographic applications. The most used models include the Bohart–Adams, Thomas, Wolborska, Yoon–Nelson, Modified dose–response, and Clark models. Generally, they have been developed to predict the breakthrough curves [13,15] neglecting biofilm dynamics. To better explore the complex relationships which establish between the biosorbent and the sorbate and elucidate the effects that the environmental or operational conditions, including the biological kinetics factors, exert on biosorption systems, more comprehensive and accurate mechanistic models need to be developed [12]. To the best of our knowledge, a first attempt on this direction has been made by the authors in [14], where a general mechanistic model accounting for the biosorption process of heavy metals on the different components (e.g. EPS, active microbial species, inert) of a multispecies biofilm has been presented. This 1D model has been conceived in the framework of continuum mathematical modeling of biofilm growth [18–20] and explicitly accounts for the diffusion and reaction of heavy metals within the biofilm matrix. The heavy metal diffusion–biosorption has been modeled by the well known diffusion–reaction equations, in which the reaction terms are functions of the number of free binding sites on the constituting biofilm components. Each biofilm component is characterized by the presence of a specific number of sorption sites, which can be free or occupied and are quantified as volume fractions. Their dynamics have been explicitly tracked. The model has been applied to a case of engineering interest which addresses the biosorption problem of a single metal on the EPS matrix of a multispecies biofilm. The model in [14] has been generalized in [21] to predict the fate of an arbitrary number of sorbates (organic/inorganic pollutants) in a biofilm system in the context of bioremediation and account for the formation of free binding sites due to biofilm expansion. The hyperbolic equations governing the dynamics of the microbial species and the free and occupied binding sites constituting the biofilm, as well as the parabolic equations for the diffusion/reaction of the dissolved substrates and sorbates have been derived from mass conservation principles in 1D and then generalized to 3D. The effects that sorbates might exert on the bacterial metabolism have been taken into account by considering a direct dependence of the growing rates on the free sorbate concentrations within the biofilm. Numerical simulations have been performed for two special cases which account for the dynamics of a free sorbate component diffusing in a multispecies biofilm and interacting with specific binding sites and the fate of two different contaminants in the same biofilm system, each of them sorbing on a specific biofilm component. However, the question of existence and uniqueness of the solutions has remained open, even in 1D case. The current paper is aimed at answering this question.

In this study, the biosorption model in [14] and its extension in [21] will be recalled and qualitatively studied. The mathematical problem is constituted by a system of nonlinear hyperbolic partial differential equations for the growth of the n microbial species constituting the biofilm, two systems of hyperbolic partial differential equations for the dynamics of the free and occupied sorption sites on the n biofilm components, a system of semilinear parabolic partial differential equations describing the diffusion and reaction of p substrates and a system of parabolic partial differential equations governing the diffusion and sorption of l sorbates. Overall this leads to a free boundary problem, essentially hyperbolic. The uniqueness and existence result to the free boundary value problem is obtained converting the differential systems to Volterra equations by introducing the characteristics lines and then using the fixed point theorem. Numerical simulations related to a special biological case where the sorbate component is acting as a stimulating agent have been performed. This is for instance the case of trace metals, which are often of vital importance for the enzyme system in bioreactors [22]. Two simulation experiments have been considered with the aim of assessing the effect of model parameters on biosorption efficiency. The work is organized as follows. In Section 2, the mathematical model is presented, the variables defined, the governing equations and the related initial and boundary conditions are introduced and discussed. In Section 3, the integral equations are derived by introducing the method of characteristics. Section 4 is devoted to the uniqueness and existence theorem. In Section 5, numerical simulations are developed for real cases of biological and engineering interest.

2. Biosorption model

2.1. Overview

In this section, the biosorption model in [14] and its extension in [21] examining the growth and sorption phenomena characterizing a multispecies biofilm proliferating in a liquid environment containing sorbates, in some cases relevant to bacterial metabolism, is studied. In the framework of 1D continuum modeling, the biofilm is assumed as a densely packed layer of bacterial cells growing mainly in the direction perpendicular to the attachment surface, with z denoting the coordinate across the surface, and constituted by n microbial species characterized by specific metabolic activities. Following Wanner and Gujer approach [18], biomass quantities are represented as microbial species concentrations $X_i(z,t)$ or equivalently as volume fractions $f_i(z,t)$, the latter indicating the fraction of available space at a particular location that is occupied by species i [23]. The biomass generated from cell growth is displaced in z direction according to a biomass advective velocity $u(z,t)$, assumed equal for all the microbial species. The location of the biofilm/liquid interface $L(t)$, herein denoted as moving boundary, is updated according to both the increased presence of biomass and the erosion of biofilm surface, usually named detachment process. The dynamics of bacterial cells inhabiting the biofilm matrix are strictly connected to nutrient (dissolved substrate) diffusion from the bulk liquid to the biofilm, which is explicitly taken into account. The bioconversion of substrates occurring within the biofilm matrix is modeled as well. The sorbate(s) is modeled as a dissolved substrate, diffusing from the bulk liquid within the biofilm matrix and enhancing or inhibiting bacterial activity based on the microbial diversity. Beyond being involved in bacterial metabolism, sorbates are subjected to sorption phenomena on the various biomass components, each one owing specific sorption features. In particular, each biofilm component is characterized by the presence of a certain number of sorption (binding) sites which are agent specific and can be categorized in two status: occupied (binded) or free. According to mass balance laws, the free and occupied binding sites are quantified as volume fractions Θ_i and $\bar{\Theta}_i$ respectively. Desorption phenomena are taken into account as well.

2.2. Free boundary value problem

The main processes related to the sorption phenomena, including biofilm and substrate dynamics, are described by the following nonlinear partial differential equations. The unknown variables that are solved for in this model and the notations used in the following equations are reported in Table 1.

$$\frac{\partial X_i}{\partial t} + \frac{\partial}{\partial z}(uX_i) = \rho_i r_{M,i}(z,t,\mathbf{X},\mathbf{S},\boldsymbol{\mu}), \quad i=1,\dots,n,\ 0 \le z \le L(t),\ t>0, \tag{2.1}$$

$$\frac{\partial u}{\partial z} = \sum_{i=1}^{n} r_{M,i}(z,t,\mathbf{X},\mathbf{S},\boldsymbol{\mu}), \quad 0 < z \le L(t),\ t \ge 0, \tag{2.2}$$

$$\dot{L}(t) = u(L(t),t) + \sigma_a(t) - \sigma_d(L(t)), \quad t>0, \tag{2.3}$$

$$\frac{\partial\ \Theta_i}{\partial t} + \frac{\partial}{\partial z}(u\Theta_i) = r_{M,i}(z,t,\mathbf{X},\mathbf{S},\boldsymbol{\mu}) + r_{\Theta,i}(z,t,\boldsymbol{\mu},\boldsymbol{\Theta},\bar{\boldsymbol{\Theta}}), \quad i=1,\dots,n, 0 \le z \le L(t),\ t>0, \tag{2.4}$$

$$\frac{\partial\ \bar{\Theta}_i}{\partial t} + \frac{\partial}{\partial z}(u\bar{\Theta}_i) = r_{\bar{\Theta},i}(z,t,\boldsymbol{\mu},\boldsymbol{\Theta},\bar{\boldsymbol{\Theta}}), \quad i=1,\dots,n,\ 0 \le z \le L(t),\ t>0, \tag{2.5}$$

$$\frac{\partial \mu_k}{\partial t} - \frac{\partial}{\partial z}\left(D_k \frac{\partial \mu_k}{\partial z}\right) = r_{\mu,k}(z,t,\mathbf{X},\mathbf{S},\boldsymbol{\mu},\boldsymbol{\Theta},\bar{\boldsymbol{\Theta}}), \quad k=1,\dots,l,\ 0 < z < L(t),\ t>0, \tag{2.6}$$

$$\frac{\partial S_j}{\partial t} - \frac{\partial}{\partial z}\left(D_{S,j} \frac{\partial S_j}{\partial z}\right) = r_{S,j}(z,t,\mathbf{X},\mathbf{S},\boldsymbol{\mu}), \quad j=1,\dots,p,\ 0 < z < L(t),\ t>0. \tag{2.7}$$

Table 1
Notations.

n	Number of microbial species
$X_i(z,t) = \rho_i f_i$	Concentration of microbial species i, $\mathbf{X} = (X_1, \dots, X_n)$
ρ_i	Constant density
$f_i(z,t)$	Volume fraction of microbial species i, $\sum_{i=1}^{n} f_i = 1$
$u(z,t)$	Advective biomass velocity
Θ_i	Volume fraction of free binding sites on microbial species i, $\boldsymbol{\Theta} = (\Theta_1, \dots, \Theta_n)$
$\bar{\Theta}_i$	Volume fraction of occupied binding sites on microbial species i, $\bar{\boldsymbol{\Theta}} = (\bar{\Theta}_1, \dots, \bar{\Theta}_n)$
l	Number of sorbates
$\mu_k(z,t)$	Concentration of sorbate k, $\boldsymbol{\mu} = (\mu_1, \dots, \mu_l)$
D_k	Diffusion coefficient of sorbate k
p	Number of substrates
$S_j(z,t)$	Concentration of substrate j, $\mathbf{S} = (S_1, \dots, S_p)$
$D_{S,j}$	Diffusion coefficient of substrate j
$r_{M,i}(z,t,\mathbf{X},\mathbf{S},\boldsymbol{\mu})$	Specific growth rate of species i
$r_{\Theta,i}(z,t,\boldsymbol{\mu},\boldsymbol{\Theta},\bar{\boldsymbol{\Theta}})$	Specific sorption/desorption rate for free binding sites on microbial species i
$r_{\bar{\Theta},i}(z,t,\boldsymbol{\mu},\boldsymbol{\Theta},\bar{\boldsymbol{\Theta}})$	Specific sorption/desorption rate for occupied binding sites on microbial species i
$r_{\mu,k}(z,t,\mathbf{X},\mathbf{S},\boldsymbol{\mu},\boldsymbol{\Theta},\bar{\boldsymbol{\Theta}})$	Reaction rate of sorbate k
$r_{S,j}(z,t,\mathbf{X},\mathbf{S},\boldsymbol{\mu})$	Production/consumption rate of substrate j
$L(t)$	Biofilm thickness, free boundary
$\sigma_a(t)$	Attachment biomass flux from bulk liquid to biofilm
$\sigma_d(L(t))$	Detachment biomass flux from biofilm to bulk liquid

The nonlinear hyperbolic partial differential equations (2.1) are derived from local mass balance and govern the dynamics of the microbial species constituting the biofilm whose spreading has been modeled as an advective transport mechanism. Beyond depending on the microbial distribution and substrate concentrations within the biofilm, the specific growth rate terms $r_{M,i}$ are functions of the sorbate trends as well, due to the influence such substances might exert on microbial metabolism (see for example metal ions etc.). Eq. (2.2) regulates the advective velocity at which the microbial mass is displaced on z direction. Such equation is obtained by summing (2.1) on i and considering the constrain $\sum_{i=1}^{n} f_i = 1$. The moving boundary evolution is governed by Eq. (2.3), which accounts for the expansion of the microbial mass and the exchanging fluxes between the biofilm and the bulk liquid, here denoted $\sigma_a(t)$ and $\sigma_d(L(t))$. The nonlinear hyperbolic partial differential equations (2.4) and (2.5) derive from local mass balance and govern the dynamics of the free and occupied binding sites respectively [21]. In particular, the reaction term $r_{M,i}$ in Eqs. (2.4) reproduces in this case the formation of free binding sites directly connected to the production of new biomass, while the term $r_{\Theta,i}$ accounts for the sorption/desorption phenomena and thus depends on the concentration of sorbate within the biofilm. Similarly, the term $r_{\bar{\Theta},i}$ represents a production/loss rate for the occupied binding sites due to sorption/desorption phenomena such that $r_{\bar{\Theta},i} = -r_{\Theta,i}$. Note that the displacement velocity for the free and occupied binding sites in Eqs. (2.4) and (2.5) is the same as the advective velocity $u(z,t)$ which regulates biofilm expansion as the sorption sites can be seen as an intrinsic characteristic of the various biofilm components. The semilinear parabolic partial differential equations (2.6) and (2.7) govern the dynamics of the sorbates and dissolved substrates which diffuse from the bulk liquid within the biofilm, where they take part to microbial metabolism or are subjected to sorption phenomena on the biofilm matrix constituents. Considering the difference in process time scales, it is common practice in biofilm modeling to assume a steady-state profile for dissolved substrate concentrations in the domain on the time scale of biomass growth [23]. Therefore, the following semilinear elliptic partial differential equations are considered for the free sorbate and substrate concentrations within the biofilm:

$$-D_k \frac{\partial^2 \mu_k}{\partial z^2} = r_{\mu,k}(z,\mathbf{X},\mathbf{S},\boldsymbol{\mu},\boldsymbol{\Theta},\bar{\boldsymbol{\Theta}}), \quad k = 1,\dots,l,\ 0 < z < L(t), \tag{2.8}$$

$$-D_{S,j} \frac{\partial^2 S_j}{\partial z^2} = r_{S,j}(z,\mathbf{X},\mathbf{S},\boldsymbol{\mu}), \quad j = 1,\dots,p,\ 0 < z < L(t). \tag{2.9}$$

2.3. Initial–boundary conditions

The following initial and boundary conditions are prescribed for the system of nonlinear partial differential equations (2.1)–(2.5) and (2.8)–(2.9).

$$X_i(z,0) = \varphi_i(z), \quad i = 1,\dots,n,\ 0 \le z \le L_0, \tag{2.10}$$

$$u(0,t) = 0, \quad t \ge 0, \qquad L(0) = L_0, \tag{2.11}$$

$$\Theta_i(z,0) = \Theta_{i0}(z), \quad \bar{\Theta}_i(z,0) = \bar{\Theta}_{i0}(z), \quad i = 1,\dots,n,\ 0 \le z \le L_0, \tag{2.12}$$

$$\frac{\partial \mu_k}{\partial z}(0,t) = 0, \qquad \mu_k(L(t),t) = \mu_{kL}(t), \quad t > 0,\ k = 1,\dots,l, \tag{2.13}$$

$$\frac{\partial S_j}{\partial z}(0,t) = 0, \qquad S_j(L(t),t) = S_{jL}(t), \quad t > 0,\ j = 1,\dots,p. \tag{2.14}$$

Eq. (2.10) designates the initial condition for X_i, with $\varphi_i(z)$ being general positive functions representing the initial biofilm composition in terms of microbial species. Condition $(2.11)_1$ for Eq. (2.2) comes from no flux condition on substratum. In Eq. $(2.11)_2$ the initial value for $L(t)$ is introduced. The functions $\Theta_{i0}(z)$ and $\bar{\Theta}_{i0}(z)$ in Eq. (2.12) designate the initial distribution of the free and occupied binding sites. For a virgin biofilm, which has not experienced sorption phenomena, the initial volume fraction of occupied binding sites for the various biofilm components can be set to zero, while $\Theta_{i0}(z)$ is assumed equal to the initial volume fraction of the ith microbial species. For $\mu_k(z,t)$, no substrate flux is assumed on the substratum $z = 0$ $(2.13)_1$ and on the free boundary $z = L(t)$ Dirichlet conditions are prescribed $(2.13)_2$. The functions $\mu_{kL}(t)$ represent the sorbate concentrations within the bulk liquid. They can be prescribed or derived from a mass balance on the liquid compartment. Similar boundary conditions are prescribed for the functions $S_j(z,t)$, where $S_{jL}(t)$ represent the substrate concentrations in the liquid environment.

3. Volterra integral equations

The partial differential equations introduced in section 2 are here converted to a system of Volterra integral equations as follows. Introducing the characteristic-like lines $z = c(z_0,t)$ defined as

$$\frac{\partial c}{\partial t}(z_0,t) = u(c(z_0,t),t), \quad c(z_0,0) = z_0,\ 0 \le z_0 \le L_0,\ t > 0, \tag{3.1}$$

and considering $(2.11)_1$, the nonlinear hyperbolic partial differential equations (2.1) are rewritten as a system of ordinary differential equations

$$\frac{d}{dt}X_i(c(z_0,t),t) = F_i(c(z_0,t),t,\mathbf{X}(c(z_0,t),t),\mathbf{S}(c(z_0,t),t),\boldsymbol{\mu}(c(z_0,t),t)), \quad 0 \le z_0 \le L_0,\ t > 0, \tag{3.2}$$

with

$$F_i = \rho_i r_{M,i}(c(z_0,t),t,\mathbf{X}(c(z_0,t),t),\mathbf{S}(c(z_0,t),t),\boldsymbol{\mu}(c(z_0,t),t)) - X_i(c(z_0,t),t)\sum_{i=1}^{n} r_{M,i}, \tag{3.3}$$

and initial conditions

$$X_i(c(z_0,0),0) = \varphi_i(z_0), \quad 0 \le z_0 \le L_0. \tag{3.4}$$

Then, the following integral equations for X_i along the characteristics are obtained

$$X_i(c(z_0,t),t) = \varphi_i(z_0) + \int_0^t F_i(c(z_0,\tau),\tau,\mathbf{X}(c(z_0,\tau),\tau),\mathbf{S}(c(z_0,\tau),\tau),\boldsymbol{\mu}(c(z_0,\tau),\tau))d\tau,$$
$$i=1,\dots,n,\ 0\le z_0\le L_0,\ t>0. \tag{3.5}$$

Similarly, the following integral equations for $\Theta_i(c(z_0,t),t)$ and $\bar{\Theta}_i(c(z_0,t),t)$ are obtained

$$\Theta_i(c(z_0,t),t) = \Theta_{i0}(z_0) + \int_0^t T_i(c(z_0,\tau),\tau,\mathbf{X}(c(z_0,\tau),\tau),\mathbf{S}(c(z_0,\tau),\tau),\boldsymbol{\mu}(c(z_0,\tau),\tau),$$
$$\boldsymbol{\Theta}(c(z_0,\tau),\tau),\bar{\boldsymbol{\Theta}}(c(z_0,\tau),\tau))d\tau,\quad i=1,\dots,n,\ 0\le z_0\le L_0,\ t>0, \tag{3.6}$$

where

$$T_i = r_{M,i}(c(z_0,\tau),\tau,\mathbf{X}(c(z_0,\tau),\tau),\mathbf{S}(c(z_0,\tau),\tau),\boldsymbol{\mu}(c(z_0,\tau),\tau))$$
$$+\ r_{\Theta,i}(c(z_0,\tau),\tau,\boldsymbol{\mu}(c(z_0,\tau),\tau),\boldsymbol{\Theta}(c(z_0,\tau),\tau),\bar{\boldsymbol{\Theta}}(c(z_0,\tau),\tau)) - \Theta_i(c(z_0,\tau),\tau)\sum_{i=1}^n r_{M,i}, \tag{3.7}$$

$$\bar{\Theta}_i(c(z_0,t),t) = \bar{\Theta}_{i0}(z_0) + \int_0^t \bar{T}_i(c(z_0,\tau),\tau,\boldsymbol{\mu}(c(z_0,\tau),\tau),\boldsymbol{\Theta}(c(z_0,\tau),\tau),\bar{\boldsymbol{\Theta}}(c(z_0,\tau),\tau))d\tau,$$
$$i=1,\dots,n,\ 0\le z_0\le L_0,\ t>0, \tag{3.8}$$

where

$$\bar{T}_i = r_{\bar{\Theta},i}(c(z_0,\tau),\tau,\boldsymbol{\mu}(c(z_0,\tau),\tau),\boldsymbol{\Theta}(c(z_0,\tau),\tau),\bar{\boldsymbol{\Theta}}(c(z_0,\tau),\tau))$$
$$-\ \bar{\Theta}_i(c(z_0,\tau),\tau)\sum_{i=1}^n r_{M,i}. \tag{3.9}$$

The following integral equation for $c(z_0,t)$ is derived from (3.1) and (2.2)

$$c(z_0,t) = z_0 + \int_0^t d\tau\int_0^{z_0}\sum_{i=1}^n r_{M,i}(c(\zeta_0,\tau),\tau,\mathbf{X}(c(\zeta_0,\tau),\tau),\mathbf{S}(c(\zeta_0,\tau),\tau),\boldsymbol{\mu}(c(\zeta_0,\tau),\tau))\frac{\partial c}{\partial\zeta_0}(\zeta_0,\tau)\ d\zeta_0,$$
$$0\le z_0\le L_0,\ t>0. \tag{3.10}$$

From (3.10) it follows easily

$$\frac{\partial c}{\partial z_0}(z_0,t) = 1 + \int_0^t\sum_{i=1}^n r_{M,i}(c(z_0,\tau),\tau,\mathbf{X}(c(z_0,\tau),\tau),\mathbf{S}(c(z_0,\tau),\tau),\boldsymbol{\mu}(c(z_0,\tau),\tau))\frac{\partial c}{\partial z_0}(z_0,\tau)d\tau. \tag{3.11}$$

The integral equations for $S_j(z,t)$ are obtained by integrating (2.9) and considering the boundary conditions $(2.14)_{2,3}$

$$S_j(z,t) = S_{jL}(t) + D_{S,j}^{-1}\int_z^L d\eta\int_0^\eta r_{S,j}(\zeta,\mathbf{X}(\zeta,t),\mathbf{S}(\zeta,t),\boldsymbol{\mu}(\zeta,t))d\zeta,$$
$$j=1,\dots,p,\quad 0<z<L(t),\ t>0. \tag{3.12}$$

Eqs. (3.12) are equivalent to the following integral equations

$$S_j(z,t) = S_{jL}(t) + D_{S,j}^{-1}\int_0^z (L-z)r_{S,j}(\zeta,\mathbf{X}(\zeta,t),\mathbf{S}(\zeta,t),\boldsymbol{\mu}(\zeta,t))d\zeta$$
$$+\ D_{S,j}^{-1}\int_z^L (L-\zeta)r_{S,j}(\zeta,\mathbf{X}(\zeta,t),\mathbf{S}(\zeta,t),\boldsymbol{\mu}(\zeta,t))d\zeta,\quad j=1,\dots,p,\quad 0<z<L(t),\ t>0. \tag{3.13}$$

Similarly, the following integral equations for μ_k are obtained

$$\mu_k(z,t) = \mu_{kL}(t) + D_k^{-1}\int_0^z (L-z) r_{\mu,k}(\zeta, \mathbf{X}(\zeta,t), \mathbf{S}(\zeta,t), \boldsymbol{\mu}(\zeta,t), \boldsymbol{\Theta}(\zeta,t), \bar{\boldsymbol{\Theta}}(\zeta,t))d\zeta$$
$$+ D_k^{-1}\int_z^L (L-\zeta) r_{\mu,k}(\zeta, \mathbf{X}(\zeta,t), \mathbf{S}(\zeta,t), \boldsymbol{\mu}(\zeta,t), \boldsymbol{\Theta}(\zeta,t), \bar{\boldsymbol{\Theta}}(\zeta,t))d\zeta,$$
$$k = 1,\dots,l, \quad 0 < z < L(t), \ t > 0. \tag{3.14}$$

The integral equation for $L(t)$ is obtained from (2.3) with initial condition $(2.11)_2$

$$L(t) = L_0 + \int_0^t u(L(\tau),\tau)\, d\tau + \int_0^t \sigma_a(\tau)\, d\tau - \int_0^t \sigma_d(L(\tau))\, d\tau, \quad t > 0. \tag{3.15}$$

4. Existence and uniqueness of solutions

An existence and uniqueness result for the integral system (3.5), (3.6), (3.8), (3.10), (3.11), (3.13), (3.14), (3.15) is derived in this section under the hypotheses $\sigma_d = \sigma_a = 0$. Note that in this case, the free boundary coincides with the characteristic line $z = c(L_0,t)$, whose evolution is governed by Eq. (3.10). In addition, considering $z = c(z_0,t)$ and introducing the change of variable $\zeta = c(\zeta_0,t), \zeta_0 < L_0$, Eqs. (3.13) and (3.14) can be written as

$$S_j(c(z_0,t),t) = S_{jL}(t)$$
$$+ D_{S,j}^{-1}\int_0^{z_0} (c(L_0,t) - c(z_0,t)) r_{S,j}(c(\zeta_0,t), \mathbf{X}(c(\zeta_0,t),t), \mathbf{S}(c(\zeta_0,t),t), \boldsymbol{\mu}(c(\zeta_0,t),t))$$
$$\times \frac{\partial c}{\partial \zeta_0}(\zeta_0,t)d\zeta_0 + D_{S,j}^{-1}\int_{z_0}^{L_0} (c(L_0,t) - \zeta_0) r_{S,j}(c(\zeta_0,t), \mathbf{X}(c(\zeta_0,t),t), \mathbf{S}(c(\zeta_0,t),t),$$
$$\boldsymbol{\mu}(c(\zeta_0,t),t)) \frac{\partial c}{\partial \zeta_0}(\zeta_0,t)d\zeta_0, \quad j = 1,\dots,m, \quad 0 < z_0 < L_0, \ t > 0. \tag{4.1}$$

$$\mu_k(c(z_0,t),t) = \mu_{kL}(t) + D_k^{-1}\int_0^{z_0} (c(L_0,t) - c(z_0,t)) r_{\mu,k}(c(\zeta_0,t), \mathbf{X}(c(\zeta_0,t),t), \mathbf{S}(c(\zeta_0,t),t),$$
$$\boldsymbol{\mu}(c(\zeta_0,t),t), \boldsymbol{\Theta}(c(\zeta_0,t),t),$$
$$\bar{\boldsymbol{\Theta}}(c(\zeta_0,t),t)) \frac{\partial c}{\partial \zeta_0}(\zeta_0,t)d\zeta_0 + D_k^{-1}\int_{z_0}^{L_0} (c(L_0,t) - \zeta_0) r_{\mu,k}(c(\zeta_0,t), \mathbf{X}(c(\zeta_0,t),t), \mathbf{S}(c(\zeta_0,t),t),$$
$$\boldsymbol{\mu}(c(\zeta_0,t),t), \boldsymbol{\Theta}(c(\zeta_0,t),t), \bar{\boldsymbol{\Theta}}(c(\zeta_0,t),t)) \frac{\partial c}{\partial \zeta_0}(\zeta_0,t)d\zeta_0, \quad k = 1,\dots,l, \ 0 < z_0 < L_0, \ t > 0. \tag{4.2}$$

By setting

$$x_i(z_0,t) = X_i(c(z_0,t),t), \quad i = 1,\dots,n, \quad \mathbf{x} = (x_1,\dots,x_n), \tag{4.3}$$

$$\vartheta_i(z_0,t) = \Theta_i(c(z_0,t),t), \quad i = 1,\dots,n, \quad \boldsymbol{\vartheta} = (\vartheta_1,\dots,\vartheta_n), \tag{4.4}$$

$$\bar{\vartheta}_i(z_0,t) = \bar{\Theta}_i(c(z_0,t),t), \quad i = 1,\dots,n, \quad \bar{\boldsymbol{\vartheta}} = (\bar{\vartheta}_1,\dots,\bar{\vartheta}_n), \tag{4.5}$$

$$s_j(z_0,t) = S_j(c(z_0,t),t), \quad j = 1,\dots,p, \quad \mathbf{s} = (s_1,\dots,s_p), \tag{4.6}$$

$$m_k(z_0,t) = \mu_k(c(z_0,t),t), \quad k = 1,\dots,l, \quad \boldsymbol{m} = (m_1,\dots,m_l), \tag{4.7}$$

and introducing the vector of unknown variables $\mathbf{x}^* = (\mathbf{x}, \boldsymbol{\vartheta}, \bar{\boldsymbol{\vartheta}}, c, \partial c/\partial z_0, \mathbf{s}, \boldsymbol{m})$ such that

$$x_i^* = x_i, \qquad x_{n+i}^* = \vartheta_i, \qquad x_{2n+i}^* = \bar{\vartheta}_i, \quad i = 1, \dots, n,$$

$$x_{3n+1}^* = c, \qquad x_{3n+2}^* = \partial c/\partial z_0, \qquad x_{3n+2+j}^* = s_j, \quad j = 1, \dots, p, \qquad x_{3n+2+p+k}^* = m_k, \quad k = 1, \dots, l.$$

the integral equations (3.5), (3.6), (3.8), (3.10), (3.11), (4.1), (4.2) are converted to the following more compact equations

$$x_i^*(z_0, t) = \varphi_i(z_0) + \int_0^t F_i(\tau, \mathbf{x}^*(z_0, \tau))d\tau, \quad i = 1, \dots, n, \ 0 \le z_0 \le L_0, \tag{4.8}$$

$$x_{n+i}^*(z_0, t) = \Theta_{i0}(z_0) + \int_0^t F_{n+i}(\tau, \mathbf{x}^*(z_0, \tau))d\tau, \quad i = 1, \dots, n, \ 0 \le z_0 \le L_0, \tag{4.9}$$

where

$$F_{n+i}(\tau, \mathbf{x}^*(z_0, \tau)) = T_i(c(z_0, \tau), \tau, \mathbf{x}(z_0, \tau), \mathbf{s}(z_0, \tau), \mathbf{m}(z_0, \tau), \boldsymbol{\vartheta}(z_0, \tau), \bar{\boldsymbol{\vartheta}}(z_0, \tau)),$$

$$x_{2n+i}^*(z_0, t) = \bar{\Theta}_{i0}(z_0) + \int_0^t F_{2n+i}(\tau, \mathbf{x}^*(z_0, \tau))d\tau, \quad i = 1, \dots, n, \ 0 \le z_0 \le L_0, \tag{4.10}$$

where

$$F_{2n+i}(\tau, \mathbf{x}^*(z_0, \tau)) = \bar{T}_i(c(z_0, \tau), \tau, \mathbf{m}(z_0, \tau), \boldsymbol{\vartheta}(z_0, \tau), \bar{\boldsymbol{\vartheta}}(z_0, \tau)),$$

$$x_{3n+1}^*(z_0, t) = z_0 + \int_0^t d\tau \int_0^{z_0} F_{3n+1}(\tau, \mathbf{x}^*(\zeta_0, \tau))d\zeta_0, \quad 0 \le z_0 \le L_0, \tag{4.11}$$

where

$$F_{3n+1}(\tau, \mathbf{x}^*(\zeta_0, \tau)) = \sum_{i=1}^{n} r_{M,i}(c(\zeta_0, \tau), \tau, \mathbf{x}(\zeta_0, \tau), \mathbf{s}(\zeta_0, \tau), \mathbf{m}(\zeta_0, \tau)) \frac{\partial c}{\partial \zeta_0}(\zeta_0, \tau),$$

$$x_{3n+2}^*(z_0, t) = 1 + \int_0^t F_{3n+2}(\tau, \mathbf{x}^*(z_0, \tau))d\tau, \quad 0 \le z_0 \le L_0, \tag{4.12}$$

where

$$F_{3n+2}(\tau, \mathbf{x}^*(z_0, \tau)) = \sum_{i=1}^{n} r_{M,i}(c(z_0, \tau), \tau, \mathbf{x}(z_0, \tau), \mathbf{s}(z_0, \tau), \mathbf{m}(z_0, \tau)) \frac{\partial c}{\partial z_0}(z_0, \tau),$$

$$x_{3n+2+j}^*(z_0, t) = S_{jL}(t) + \int_0^{z_0} F_{3n+2+j}^1(\mathbf{x}^*(\zeta_0, t))d\zeta_0 + \int_{z_0}^{L_0} F_{3n+2+j}^2(\mathbf{x}^*(\zeta_0, t))d\zeta_0,$$
$$j = 1, \dots, p, \ 0 < z_0 < L_0, \tag{4.13}$$

where

$$F_{3n+2+j}^1(\mathbf{x}^*(\zeta_0, t)) = D_{S,j}^{-1}(x_{3n+1}^*(L_0, t) - x_{3n+1}^*(z_0, t)) r_{S,j}(x_{3n+1}^*(\zeta_0, t), \mathbf{x}(\zeta_0, t), \mathbf{s}(\zeta_0, t), \mathbf{m}(\zeta_0, t)) \frac{\partial c}{\partial \zeta_0}(\zeta_0, t),$$

$$F_{3n+2+j}^2(\mathbf{x}^*(\zeta_0, t)) = D_{S,j}^{-1}(x_{3n+1}^*(L_0, t) - \zeta_0) r_{S,j}(x_{3n+1}^*(\zeta_0, t), \mathbf{x}(\zeta_0, t), \mathbf{s}(\zeta_0, t), \mathbf{m}(\zeta_0, t)) \frac{\partial c}{\partial \zeta_0}(\zeta_0, t),$$

$$x_{3n+2+p+k}^*(z_0, t) = \mu_{jL}(t) + \int_0^{z_0} F_{3n+2+m+k}^1(\mathbf{x}^*(\zeta_0, t))d\zeta_0 + \int_{z_0}^{L_0} F_{3n+2+m+k}^2(\mathbf{x}^*(\zeta_0, t))d\zeta_0,$$
$$k = 1, \dots, l, \ 0 < z_0 < L_0, \tag{4.14}$$

where

$$F^1_{3n+2+p+k}(\mathbf{x}^*(\zeta_0,t)) = D_k^{-1}(x^*_{3n+1}(L_0,t) - x^*_{3n+1}(z_0,t))r_{\mu,k}(x^*_{3n+1}(\zeta_0,t), \mathbf{x}(\zeta_0,t), \mathbf{s}(\zeta_0,t), \mathbf{m}(\zeta_0,t), \boldsymbol{\vartheta}(\zeta_0,t), \bar{\boldsymbol{\vartheta}}(\zeta_0,t))\frac{\partial c}{\partial \zeta_0}(\zeta_0,t),$$

$$F^2_{3n+2+p+k}(\mathbf{x}^*(\zeta_0,t)) = D_k^{-1}(x^*_{3n+1}(L_0,t) - \zeta_0)r_{\mu,k}(x^*_{3n+1}(\zeta_0,t), \mathbf{x}(\zeta_0,t), \mathbf{s}(\zeta_0,t), \mathbf{m}(\zeta_0,t), \boldsymbol{\vartheta}(\zeta_0,t), \bar{\boldsymbol{\vartheta}}(\zeta_0,t))\frac{\partial c}{\partial \zeta_0}(\zeta_0,t).$$

Consider the map $\mathbf{y} = A\mathbf{x}^*$, where $A(\mathbf{x}^*)$ designates the right hand side of Eqs. (4.8)–(4.14). Denote by $\mathbf{V}$ the vector space of the continuous functions $x^*_h,\ h = 1,\dots,3n+2+p+l$, on $I = [0, L_0] \times [0, T]$. The following results can be proved.

Lemma. *Assume that:*

(i) *The functions $x^*_h(z_0,t)$ are continuous on $C(I), I = [0,L_0]\times[0,T_1], L_0 > 0, T_1 > 0,\ h = 1,\dots,3n+2+p+l$;*

(ii) *$\varphi_i(z_0), \Theta_{i0}(z_0), \bar{\Theta}_{i0}(z_0)$ are positive continuous functions on $C(I), I = [0,L_0]\times[0,T_1], L_0 > 0, T_1 > 0,\ i = 1,\dots,n$;*

(iii) *$S_{jL},\ j = 1,\dots,p$ and $\mu_{kL},\ k = 1,\dots,l$ are positive continuous functions;*

(iv) *$|x^*_i - \varphi_i| \le K_i,\ i = 1,\dots,n$; $|x^*_{n+i} - \Theta_{i0}| \le K_{n+i},\ i = 1,\dots,n$; $|x^*_{2n+i} - \bar{\Theta}_{i0}| \le K_{2n+i},\ i = 1,\dots,n$; $|x^*_{3n+1} - z_0| \le K_{3n+1}$; $1 \le x^*_{3n+2} \le 1 + K_{3n+2}$; $|x^*_{3n+2+j} - S_{jL}| \le K_{3n+2+j},\ j = 1,\dots,p$; $|x^*_{3n+2+p+k} - \mu_{jL}| \le K_{3n+2+p+k},\ k = 1,\dots,l$, where $K_h = constant > 0$;*

(v) *$G = \sum_{i=1}^n (r_{M,i}(c(z_0,t),t,\mathbf{x}(z_0,t),\mathbf{s}(z_0,t),\mathbf{m}(z_0,t)))$ is essentially positive;*

(vi) *F_h are continuous and bounded functions with*

$$M_h = \max|F_h|, \quad h = 1,\dots,3n+2,$$

$$M^1_{3n+2+j} = \max|F^1_{3n+2+j}|, \qquad M^2_{3n+2+j} = \max|F^2_{3n+2+j}|,$$
$$M_{3n+2+j} = \max\{M^1_{3n+2+j}, M^2_{3n+2+j}\}, \quad j = 1,\dots,p,$$

$$M^1_{3n+2+p+k} = \max|F^1_{3n+2+p+k}|, \qquad M^2_{3n+2+p+k} = \max|F^2_{3n+2+p+k}|,$$
$$M_{3n+2+p+k} = \max\{M^1_{3n+2+p+k}, M^2_{3n+2+p+k}\}, \quad k = 1,\dots,l,$$

when $(z_0,t) \in [0,\ L_0]\times[0,\ T_1]$ and the functions x^*_h satisfy the assumptions (i)–(v). *Under the hypotheses* (i)–(vi) *A maps V into itself.*

Proof. Consider

$$T = \min\left\{T_1, \frac{K_1}{M_1}, \dots, \frac{K_{3n}}{M_{3n}}, \frac{K_{3n+1}}{L_0 M_{3n+2}}, \frac{K_{3n+2}}{M_{3n+2}}\right\}.$$

Let $K_{3n+2+j} = 2M_{3n+2+j}L_0$ and $K_{3n+2+p+k} = 2M_{3n+2+p+k}L_0$. Firstly, hypothesis (v), jointly with $x^*_{3n+2} \ge 1$, implies $F_{3n+2} \ge 0$.

Then,

$$|x^*_i - \varphi_i| \le M_i T \le K_i, \quad i = 1,\dots,n,$$

$$|x^*_{n+i} - \Theta_{i0}| \le M_i T \le K_{n+i}, \quad i = 1,\dots,n,$$

$$|x^*_{2n+i} - \bar{\Theta}_{i0}| \le M_i T \le K_{2n+i}, \quad i = 1, \dots, n,$$
$$|x^*_{3n+1} - z_0| \le M_{3n+1} T L_0 \le K_{3n+1},$$
$$1 \le x^*_{3n+2} \le 1 + M_{3n+2} T \le 1 + K_{3n+2},$$
$$|x^*_{3n+2+j} - S_{jL}| \le 2M_{3n+2+j} L_0 \le K_{3n+2+j}, \quad j = 1, \dots, p,$$
$$|x^*_{3n+2+p+k} - \mu_{jL}| \le 2M_{3n+2+p+k} L_0 \le K_{3n+2+p+k}, \quad k = 1, \dots, l,$$

which is the desired result.

Theorem. *Under the same hypotheses as the Lemma there exists a unique continuous solution* $x^*_h(z_0, t), h = 1, \dots, 3n + 2 + p + l,\ 0 \le z_0 \le L_0,\ 0 \le t \le T$ *to system* (4.8)–(4.14).

Proof. Consider $\tilde{x}^* \in \mathbf{V}$ with $\tilde{y} = A\tilde{x}^*$. In the Lemma, it has been shown that A maps V into itself. Let us now prove that A is a contractive map.

Assume F_h Lipschitz continuous functions with respect to $x^*_h, h = 1, \dots, 3n + 2 + p + l$

$$|F_i(\tau, \mathbf{x}^*) - F_i(\tau, \tilde{\mathbf{x}}^*)| \le \lambda_i \sum_{h=1}^{3n+2+p+l} |x^*_h - \tilde{x}^*_h|, \quad i = 1, \dots, 3n + 2,$$
$$|F^1_i(\tau, \mathbf{x}^*) - F^1_i(\tau, \tilde{\mathbf{x}}^*)| \le \lambda^1_i \sum_{h=1}^{3n+2+p+l} |x^*_h - \tilde{x}^*_h|, \quad i = 3n + 3, \dots, 3n + 2 + p + l,$$
$$|F^2_i(\tau, \mathbf{x}^*) - F^2_i(\tau, \tilde{\mathbf{x}}^*)| \le \lambda^2_i \sum_{h=1}^{3n+2+p+l} |x^*_h - \tilde{x}^*_h|, \quad i = 3n + 3, \dots, 3n + 2 + p + l.$$

and introduce the norm

$$\|\mathbf{x}^*\| = \sum_{h=1}^{3n+2+p+l} \max_I \exp(-\gamma t)|x^*_h|,$$

with γ a positive constant.

It follows:

$$|y_i - \tilde{y}_i| \exp(-\gamma t) \le (\lambda_i/\gamma)\|\mathbf{x}^* - \tilde{\mathbf{x}}^*\|, \quad i = 1, \dots, 3n,$$
$$|y_{3n+1} - \tilde{y}_{3n+1}| \exp(-\gamma t) \le (\lambda_{n+1} L_0/\gamma)\|\mathbf{x}^* - \tilde{\mathbf{x}}^*\|,$$
$$|y_{3n+2} - \tilde{y}_{3n+2}| \exp(-\gamma t) \le (\lambda_{n+2}/\gamma)\|\mathbf{x}^* - \tilde{\mathbf{x}}^*\|,$$
$$|y_i - \tilde{y}_i| \exp(-\gamma t) \le (\lambda^1_i + \lambda^2_i) L_0 \|\mathbf{x}^* - \tilde{\mathbf{x}}^*\|, \quad i = 3n + 3, \dots, 3n + 2 + p + l,$$

Hence,

$$\|\mathbf{y}^* - \tilde{\mathbf{y}}^*\| \le \Lambda \|\mathbf{x}^* - \tilde{\mathbf{x}}^*\|,$$

where

$$\Lambda = \Lambda_1 + \Lambda_2,$$
$$\Lambda_1 = \frac{1}{\gamma}\left(\sum_{i=1}^{3n} \lambda_i + \lambda_{3n+1} L_0 + \lambda_{3n+2}\right), \qquad \Lambda_2 = L_0 \sum_{i=3n+3}^{3n+2+p+l} (\lambda^1_i + \lambda^2_i).$$

Selecting γ such that $\Lambda_1 < \epsilon$, $\forall \epsilon > 0$ and L_0 small enough such that

$$L_0 \le (1 - \epsilon)\left(\sum_{i=3n+3}^{3n+2+p+l} (\lambda^1_i + \lambda^2_i)\right)^{-1},$$

then, $\Lambda < 1$ and the theorem is proved.

5. Numerical applications to a heterotrophic–autotrophic biofilm system for wastewater treatment

In this section, we consider numerical solutions to the free boundary problem stated above. The numerical analysis has been developed by using the method of characteristics as in [24,25] and an original software has been properly set-up. Accuracy was checked by comparison to the equation $\sum_{i=1}^{n} f_i(z,t) = 1$. The mathematical model presented in its general form in Section 2 has been applied to the well-known case of a heterotrophic–autotrophic biofilm growing in a liquid environment and devoted to wastewater treatment [26]. The biofilm is supposed to act as a biosorbent for the entrapment of heavy metals in trace concentration. Beyond being involved in sorption processes, the heavy metals might operate as stimulating or inhibiting agents for the biofilm metabolism itself, as reported in [22]. Two microbial species are considered: heterotrophic bacteria $X_1 = \rho_1 f_1$ using organic carbon S_1 as substrate and autotrophic bacteria $X_2 = \rho_2 f_2$ growing on ammonium S_2 as substrate. The decay of these microbial species produces residual inert microbial biomass, which is treated as an additional particulate component $X_3 = \rho_3 f_3$. Extracellular polymeric substances (EPS) $X_4 = \rho_4 f_4$ production has been also taken into account following the unified theory for microbial products developed in [27]. Four reacting components are simultaneously considered: organic carbon S_1, expressed in terms of COD, ammonium S_2, oxygen S_3 and the heavy metal μ_1. Oxygen is used for ammonium and organic carbon oxidation. Ammonium, organic carbon and oxygen are provided from the bulk liquid at a constant concentration. The heavy metal concentration within the liquid environment is supposed constant on time as well. The biomass increase is determined by the metabolism of the dissolved components. In particular, the autotrophic bacteria X_2 metabolize ammonium S_2 while the heterotrophs X_1 consume organic carbon S_1. Both microbial groups use oxygen S_3 as electron acceptor. The heavy metal μ_1 has been considered as a co-substrate for the microbial metabolism of both heterotrophic and autotrophic bacteria. Moreover, the biosorption process has been considered irreversible and selective for the binding sites present on biomass component X_1. The biofilm growth is governed by Eqs. (2.1), rewritten here in terms of bacterial volume fractions for convenience

$$\frac{\partial f_i}{\partial t} + \frac{\partial}{\partial z}(u f_i) = r_{M,i}(z,t,\mathbf{X},\mathbf{S},\boldsymbol{\mu}), \quad i = 1,\dots,4,\ 0 \le z \le L(t),\ t > 0. \tag{5.1}$$

The biomass growth rates are expressed as:

$$r_{M,1} = ((1-k_1)m_1^*(\mathbf{S},\boldsymbol{\mu}) - c_1)f_1, \tag{5.2}$$

$$r_{M,2} = ((1-k_2)m_2^*(\mathbf{S},\boldsymbol{\mu}) - c_2)f_2, \tag{5.3}$$

while for inert residues

$$r_{M,3} = c_1 f_1 + c_2 f_2, \tag{5.4}$$

and EPS

$$r_{M,4} = k_1 m_1^* f_1 + k_2 m_2^* f_2, \tag{5.5}$$

where m_1, m_2, are the net biomass growth rates for biomass X_1, X_2; c_1 and c_2 are the decay rates for the heterotrophic and autotrophic microorganisms; k_1 and k_2 are the growth-associated EPS formation coefficients.

The net biomass growth rates are given by:

$$m_1^* = \mu_{\max,1}\frac{S_1}{K_{1,1}+S_1}\frac{S_3}{K_{1,3}+S_3}\frac{\mu_1}{K_{\mu,1}+\mu_1}, \tag{5.6}$$

$$m_2^* = \mu_{\max,2}\frac{S_2}{K_{2,2}+S_2}\frac{S_3}{K_{2,3}+S_3}\frac{\mu_1}{K_{\mu,2}+\mu_1}, \tag{5.7}$$

Table 2
Parameter values used for numerical simulations.

Parameter	Symbol	Unit	Value	Reference
Maximum growth rate of X_1	$\mu_{\max,1}$	d^{-1}	4.8	[18]
Maximum growth rate of X_2	$\mu_{\max,2}$	d^{-1}	0.95	[18]
Half saturation constant of X_1 on S_1	$K_{1,1}$	mg/L	5	[18]
Half saturation constant of X_1 on S_3	$K_{1,3}$	mg/L	0.1	[18]
Half saturation constant of X_2 on S_2	$K_{2,2}$	mg/L	1	[18]
Half saturation constant of X_2 on S_3	$K_{2,3}$	mg/L	0.1	[18]
Half saturation constant of X_1 on μ_1	$K_{\mu,1}$	mg/L	10^{-7}	This study
Half saturation constant of X_2 on μ_1	$K_{\mu,2}$	mg/L	10^{-7}	This study
Yield of X_1 on S_1	Y_1	$g_{biomass}/g_{substrate}$	0.4	[18]
Yield of X_2 on S_2	Y_2	$g_{biomass}/g_{substrate}$	0.22	[18]
Yield of X_1 on μ_1	$Y_{\mu,1}$	$g_{biomass}/g_{substrate}$	10^5	This study
Yield of X_2 on μ_1	$Y_{\mu,2}$	$g_{biomass}/g_{substrate}$	10^5	This study
Microbial decay constant of X_1	c_1	d^{-1}	0.05	[27]
Microbial decay constant of X_2	c_2	d^{-1}	0.05	This study
Growth-associated EPS formation coefficient for X_1	k_1	–	0.663	This study
Growth-associated EPS formation coefficient for X_2	k_2	–	0.663	This study
Biosorption yield of μ_1 on X_1	Y_{ads}	g_{metal}/n_{sites}	1	This study
Erosion parameter	λ	$m^{-1}d^{-1}$	1250	This study

Table 3
Initial–boundary conditions used for numerical simulations.

Parameter	Symbol	Unit	Value
Initial Biofilm thickness	L_0	μm	300
Initial Volume Fraction of f_1	$f_1(z,0)$	–	0.4
Initial Volume Fraction of f_2	$f_2(z,0)$	–	0.5
Initial Volume Fraction of f_3	$f_3(z,0)$	–	0.0
Initial Volume Fraction of f_4	$f_4(z,0)$	–	0.1
Initial concentration of S_1	$S_{1,0}(z)$	mg/L	0.0
Initial concentration of S_2	$S_{2,0}(z)$	mg/L	0.0
Initial concentration of S_3	$S_{3,0}(z)$	mg/L	0.0
Initial concentration of μ_1	$\mu_{1,0}(z)$	mg/L	0.0
S_1 concentration at $z = L$	S_{1L}	mg/L	20.0
S_2 concentration at $z = L$	S_{2L}	mg/L	2.0
S_3 concentration at $z = L$	S_{3L}	mg/L	8.0
μ_1 concentration at $z = L$	μ_{1L}	mg/L	$4 * 10^{-4}$

where $\mu_{\max,i}$ denotes the maximum net growth rate for biomass i, $K_{i,j}$ the affinity constant of substrate j for biomass i, $K_{\mu,i}$ the half saturation constant of species i for μ_1. The values assumed for the former parameters in the numerical simulations are taken from the literature and are reported in Table 2.

The following initial conditions will be considered for Eqs. (5.1)

$$f_i(z,0) = f_{i,0}(z), 0 \le z \le L_0, \quad i = 1,2,3,4. \tag{5.8}$$

The functions $f_{i,0}(z)$, $i = 1,\dots,4$, represent the initial volume fractions of biofilm components and their values are reported in Table 3.

The reaction rate for Θ_1 in Eqs. (2.4) accounts for a non-reversible mechanism of metal sorption on the component X_1 and is expressed as

$$r_{\Theta,1} = -k_{ads}\mu_1\Theta_1, \tag{5.9}$$

with k_{ads} being the sorption constant for the heavy metal μ_1 on biomass component X_1, whose value is reported in Table 2. As above mentioned, the production rate for the volume fraction of occupied binding sites $r_{\bar{\Theta},1}$ is the opposite of $r_{\Theta,1}$. Moreover, the sorption rates for all the other biomass components $r_{\Theta,i}, i = 2,\dots,4$ have been set to zero. Similarly to f_i, the following initial conditions have been set to Θ_i

$$\Theta_i(z,0) = \Theta_{i,0}(z) = f_{i,0}(z), 0 \le z \le L_0, \quad i = 1,2,3,4. \tag{5.10}$$

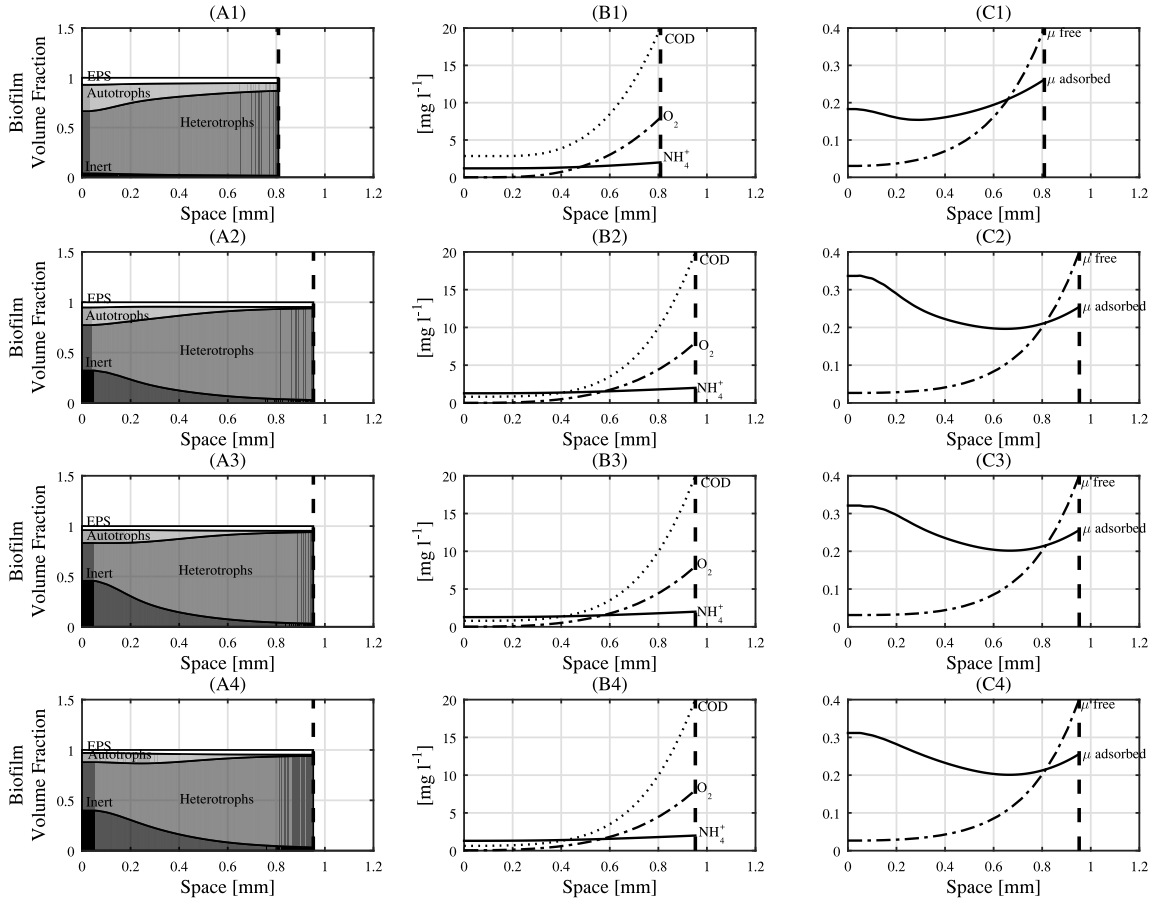

Fig. 5.1. Microbial species distribution (A1, A2, A3, A4), substrate trends (B1, B2, B3, B4), free and adsorbed heavy metal concentrations (C1, C2, C3, C4) after 1, 10, 20 and 100 days simulation time within a heterotrophic–autotrophic biofilm system devoted to wastewater treatment ($k_{ads} = 5 * 10^3$, $N_1 = 1$). μ_1 concentration is multiplied by a factor of 10^3.

Organic carbon, ammonium and oxygen dynamics are governed by Eqs. (2.7), where the net conversion rates $r_{S,j}(z, t, \mathbf{X}, \mathbf{S}, \boldsymbol{\mu})$ for substrate $j = 1, 2, 3$ are expressed by:

$$r_{S,1} = -\frac{1}{Y_1} m_1^* X_1, \tag{5.11}$$

$$r_{S,2} = -\frac{1}{Y_2} m_2^* X_2, \tag{5.12}$$

$$r_{S,3} = -(1 - k_1)\frac{(1 - Y_1)}{Y_1} m_1^* X_1 - (1 - k_2)\frac{(1 - Y_2)}{Y_2} m_2^* X_2, \tag{5.13}$$

where Y_i denotes the yield for biomass i (Table 2). The following initial–boundary conditions will be considered for Eqs. (2.7)

$$S_j(z, 0) = S_{j0}(z), \quad 0 \le z \le L_0, \ j = 1, 2, 3 \tag{5.14}$$

$$\frac{\partial S_j}{\partial z}(0, t) = 0, \qquad S_j(L(t), t) = S_{jL}, \quad 0 < t \le T, \tag{5.15}$$

where S_{jL} denotes the constant ammonium, organic carbon and oxygen level within the bulk liquid, whose value is reported in Table 3.

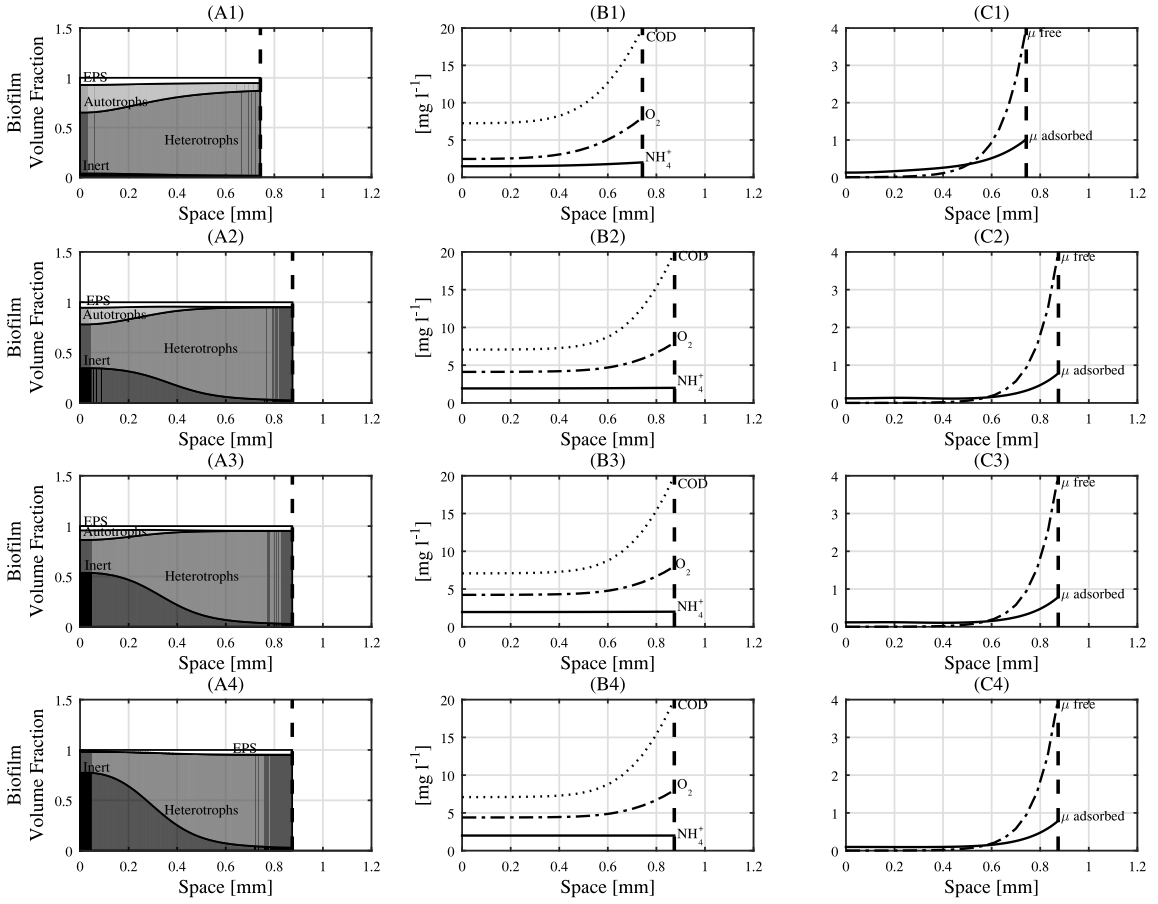

Fig. 5.2. Microbial species distribution (A1, A2, A3, A4), substrate trends (B1, B2, B3, B4), free and adsorbed heavy metal concentrations (C1, C2, C3, C4) after 1, 10, 20 and 100 days simulation time within a heterotrophic–autotrophic biofilm system devoted to wastewater treatment ($k_{ads} = 5 * 10^3$, $N_1 = 5$). μ_1 concentration is multiplied by a factor of 10^4.

The heavy metal dynamics are governed by Eq. (2.6), where the net consumption rate $r_{\mu,1}$ can be expressed as:

$$r_{\mu,1} = -\frac{m_1^*}{Y_{\mu,1}} X_1 - \frac{m_2^*}{Y_{\mu,2}} X_2 - Y_{ads} N_1 k_{ads} \mu_1 \Theta_1, \tag{5.16}$$

where $Y_{\mu,i}$ denotes the yield of biomass X_i on the heavy metal μ_1, N_1 the concentration of sorption sites on biomass component X_1 and Y_{ads} the biosorption yield expressed in terms of grams of heavy metal on number of sites (Table 2).

The following initial–boundary conditions will be considered for Eqs. (2.6)

$$\mu_1(z,0) = 0, \quad 0 \le z \le L_0, \tag{5.17}$$

$$\frac{\partial \mu_k}{\partial z}(0,t) = 0, \qquad \mu_k(L(t),t) = \mu_{kL}, \quad 0 < t \le T, \tag{5.18}$$

where μ_{kL} denotes the heavy metal concentration in the bulk liquid, assumed constant over time and whose value is reported in Table 3.

Biosorption efficiency is significantly influenced by many parameters such as environmental factors, the sorbing material and the metal species to be removed, and highly depends on the type of microbial cultures

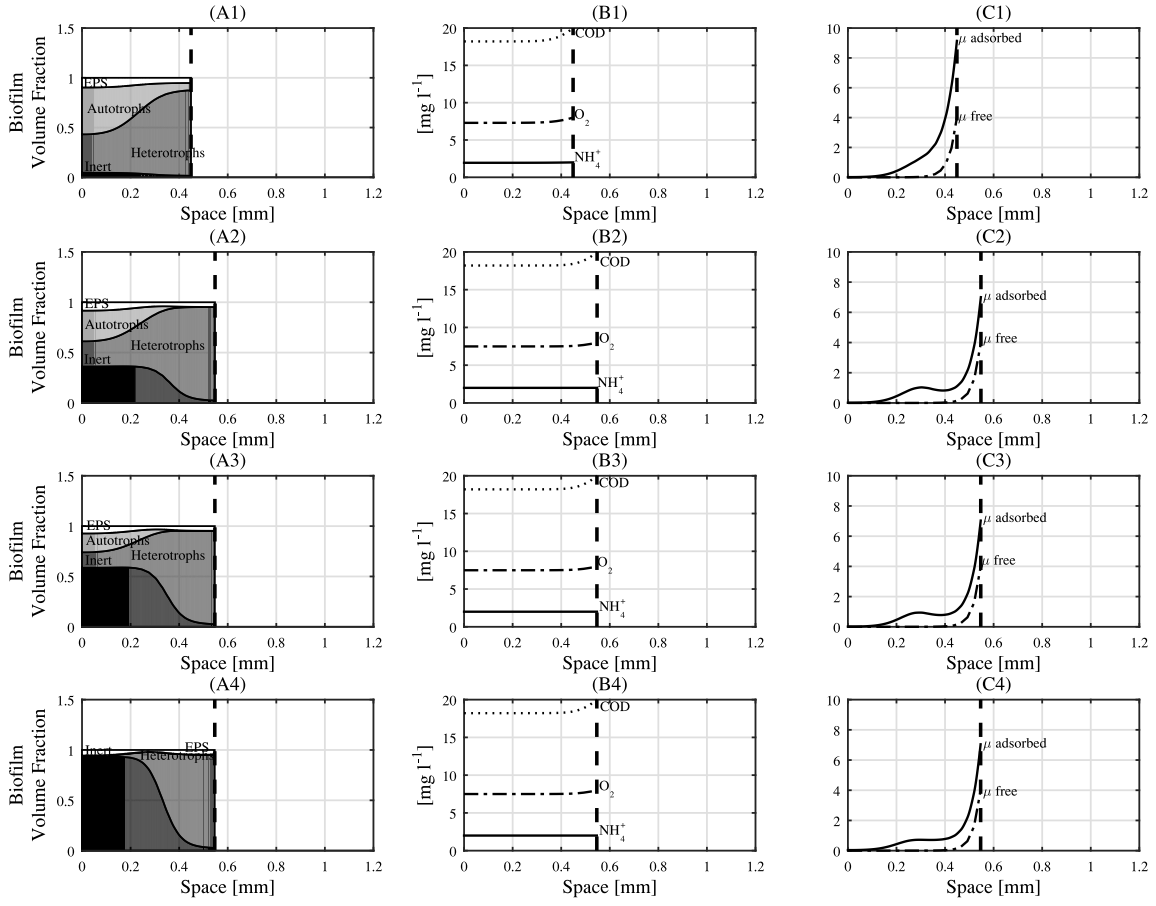

Fig. 5.3. Microbial species distribution (A1, A2, A3, A4), substrate trends (B1, B2, B3, B4), free and adsorbed heavy metal concentrations (C1,C2,C3,C4) after 1, 10, 20 and 100 days simulation time within a heterotrophic–autotrophic biofilm system devoted to wastewater treatment ($k_{ads} = 5 * 10^3$, $N_1 = 50$). μ_1 concentration is multiplied by a factor of 10^4.

involved. In this context, the main goals for the computational studies are to determine how successful biosorption depends on some parameters of the system. For this reason we vary the density of binding sites N_1 on X_1 and the sorption constant k_{ads} and we use the term sites density to refer to the applications with a variable sorption sites density but constant k_{ads} and the phrase sorption constant to refer to the second protocol. A summarizing panel of the numerical simulations with the relative value associated to the constants N_1 and k_{ads} is reported in Table 4.

Table 4
Summary of the simulation studies.

STUDY I		STUDY II	
Set #	N_1	Set #	k_{ads}
1.1	1	2.1	$5 * 10^4$
1.2	5	2.2	$5 * 10^2$
1.3	50	2.3	5
1.4	500		
$k_{ads} = 5 * 10^3$		$N_1 = 2$	

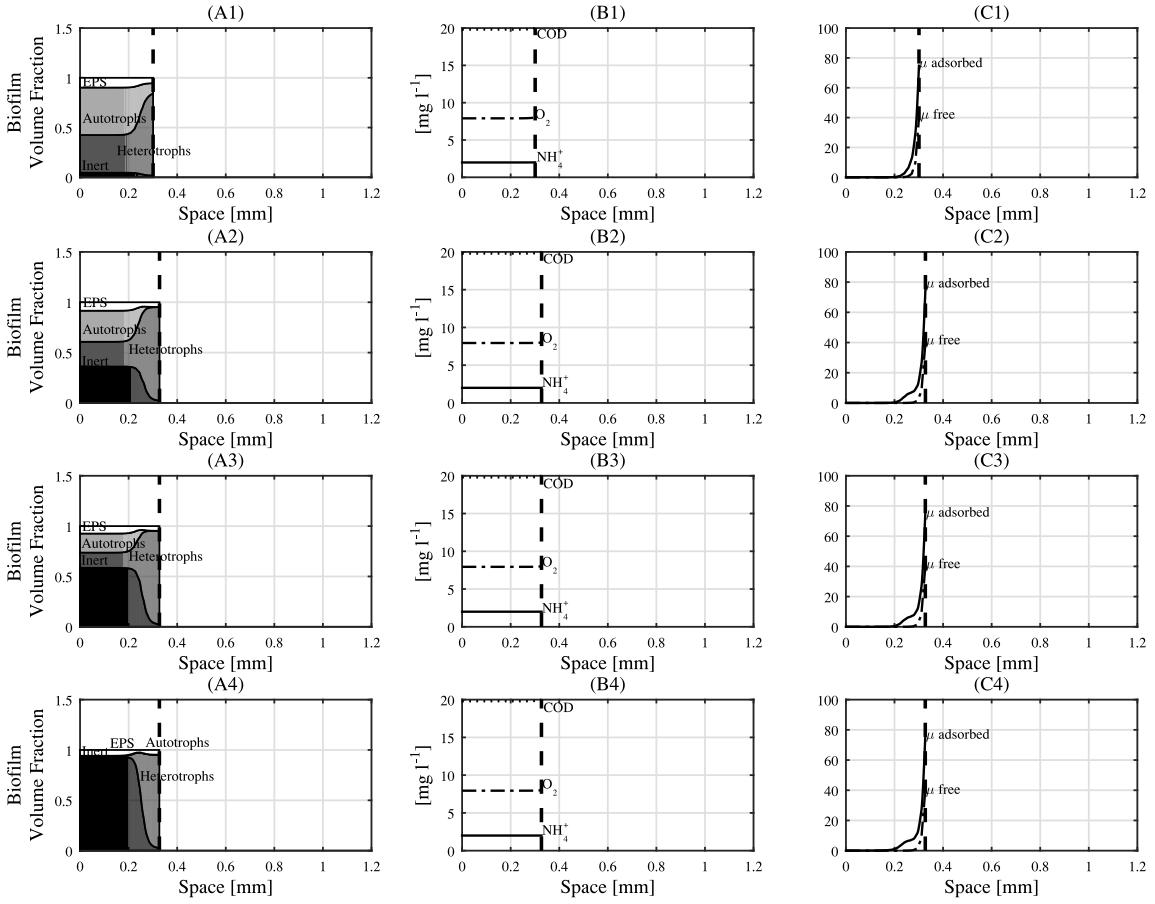

Fig. 5.4. Microbial species distribution (A1, A2, A3, A4), substrate trends (B1, B2, B3, B4), free and adsorbed heavy metal concentrations (C1, C2, C3, C4) after 1, 10, 20 and 100 days simulation time within a heterotrophic–autotrophic biofilm system devoted to wastewater treatment ($k_{ads} = 5 * 10^3$, $N_1 = 500$). μ_1 concentration is multiplied by a factor of 10^5.

5.1. Study I: sites density

Model outcomes for each simulation experiment have been summarized in Figs. 5.1–5.4. More precisely, simulation results have been reported for each investigated biofilm system in terms of microbial species distribution, substrate concentration trends, free and sorbed heavy metal within the biofilm for each specific simulation time. In Fig. 5.1(A1, A2, A3, A4) a reduction in microbial diversity occurs: X_2 which are initially present within the biofilm are outcompeted by X_1 due to the higher growth rate and the heavy metal limitation. Indeed, after 100 days simulation time (Fig. 5.1(A4)) X_1 represent the most abundant microbial species all over the biofilm, while X_2 occupy the inner part of the biofilm. Due to microbial decay, the inert concentration increases over time, reaching the highest concentration close to the substratum. For what concerns substrate profiles, S_1 is found to decrease within the biofilm due to the microbial metabolism; S_2 is mostly consumed during the first simulation days due to the higher X_2 concentration while it keeps almost constant when the microbial diversity decreases (Fig. 5.1(B1, B2, B3, B4)). S_3 drops to zero in the inner part of the biofilm. The heavy metal μ_1 shows a fully penetrated profile: it acts as a stimulating agent for both X_1 and X_2 metabolisms and adsorbs progressively on X_1. The concentration of the sorbed heavy metal is reported in Fig. 5.1(C1, C2, C3, C4) as well. In Figs. 5.2–5.4(A1, A2, A3, A4), it is possible to note that a higher N_1 leads to the complete loss of X_2 and a reduced biofilm thickness. In particular, Fig. 5.2(A4) shows that after 100 days simulation time the biofilm is essentially constituted by X_1, X_3 and X_4, the latter

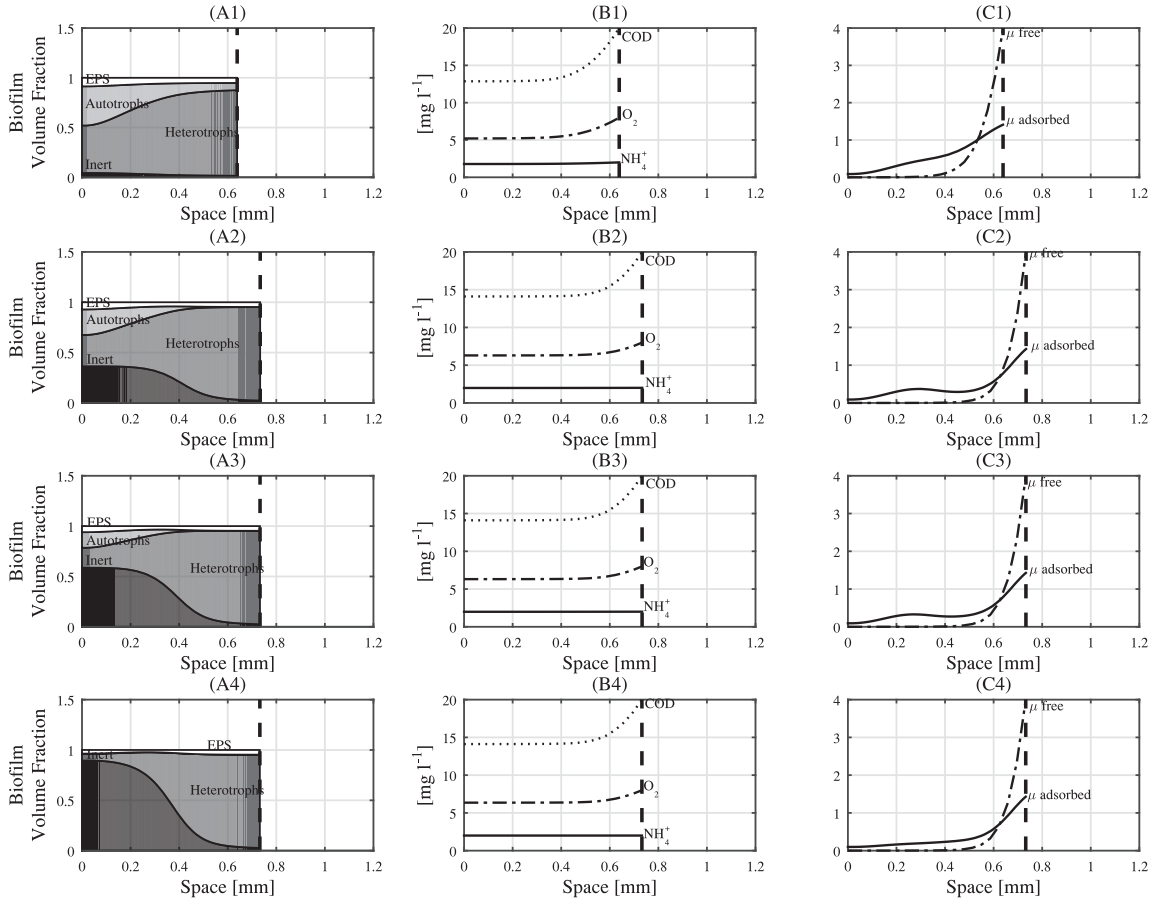

Fig. 5.5. Microbial species distribution (A1, A2, A3, A4), substrate trends (B1, B2, B3, B4), free and adsorbed heavy metal concentrations (C1, C2, C3, C4) after 1, 10, 20 and 100 days simulation time within a heterotrophic–autotrophic biofilm system devoted to wastewater treatment ($k_{ads} = 5 * 10^4$, $N_1 = 2$). μ_1 concentration is multiplied by a factor of 10^4.

in small concentration in the outmost part of the biofilm. S_1 and S_3 show a fully penetrated profile while S_2 remains constant after 10 days simulation time (Fig. 5.2(B1, B2, B3, B4)). The heavy metal concentration drops to zero in the middle of the biofilm matrix as it progressively adsorbs on the outmost part of the biofilm where it is contemporarily used for X_1 metabolism (Fig. 5.2(C1, C2, C3, C4)). The lack of heavy metal in the inner part of the biofilm represents one of the cues inducing the loss of X_2, as μ_1 acts as a stimulating agent for both X_1 and X_2. The sorbed heavy metal concentration keeps higher in the outmost part of the biofilm for all the simulation times (Fig. 5.2(C1, C2, C3, C4)). For $N_1 = 50$ and $N_1 = 500$, a similar trend can be observed. However, when N_1 increases, biofilm thickness decreases as μ_1 concentration drops to zero in the outmost part of the biofilm as a consequence of the progressive sorption on the heterotrophic biofilm fraction (Figs. 5.3–5.4). X_2 are completely out-competed after 100 days simulation time (Figs. 5.3–5.4(A4)), while X_1, which initially occupy the whole biofilm matrix, start to proliferate over time only in the outmost part of the biofilm, where there is nutrient abundance and heavy metal availability (Figs. 5.3–5.4(A1, A2, A3, A4)). After 100 days simulation time, the biofilm is so partitioned: the outmost part is microbially active while the inner part is mainly constituted by inert material, which derives from the bacterial decay (Figs. 5.3–5.4(A1, A2, A3, A4)). For what concerns substrate profiles, for both the simulation *set* 1.3 and *set* 1.4 $S_j, j = 1, \ldots, 3$ show a fully penetrated profile. In particular, S_2 keeps constant for all the simulation times; S_1 and S_3 are slightly consumed due to the reduced X_1 concentration within the biofilm matrix (Figs.

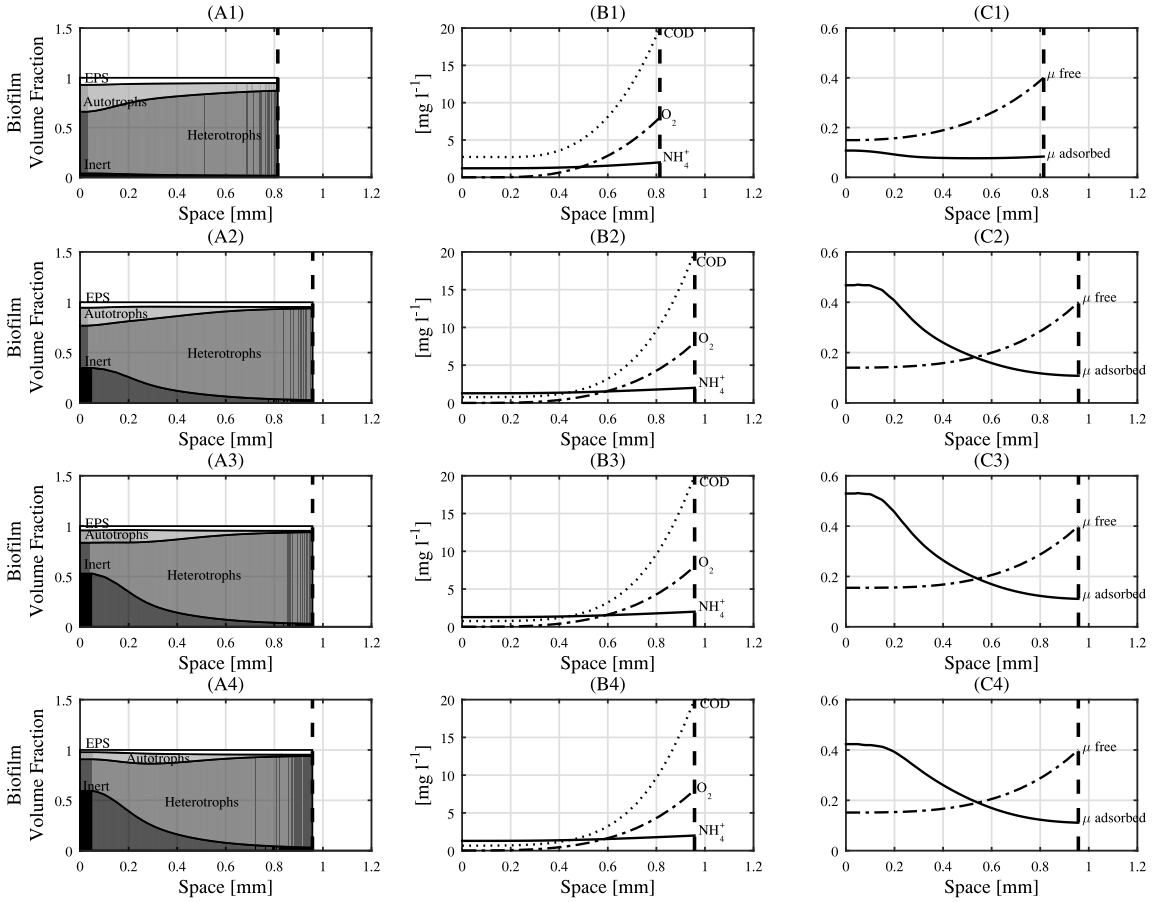

Fig. 5.6. Microbial species distribution (A1, A2, A3, A4), substrate trends (B1, B2, B3, B4), free and adsorbed heavy metal concentrations (C1, C2, C3, C4) after 1, 10, 20 and 100 days simulation time within a heterotrophic–autotrophic biofilm system devoted to wastewater treatment ($k_{ads} = 5 * 10^2$, $N_1 = 2$). μ_1 concentration is multiplied by a factor of 10^3.

5.3–5.4(B1, B2, B3, B4)). The heavy metal adsorbs progressively in the outmost part of the biofilm where the highest concentration of sorbed heavy metal can be also found (Figs. 5.3–5.4(C1, C2, C3, C4)).

5.2. Study II: biosorption constant

Simulation study II analyzes the effect of k_{ads} on biosorption efficiency and biofilm dynamics. Similarly to the previous numerical experiment, model outcomes for each simulation experiment have been summarized in Figs. 5.5–5.7, where the microbial species distribution, substrate concentration trends, free and sorbed heavy metal within the biofilm for each specific biofilm system and simulation time have been reported. In Fig. 5.5 simulation results for the highest biosorption constant have been summarized. Microbial diversity is found again to decrease over time and X_2 is completely outcompeted after 100 days simulation time (Fig. 5.5(A1, A2, A3, A4)). The biofilm is essentially constituted by X_1, which proliferates thanks to the nutrient abundance and heavy metal availability in the outmost part of the biofilm, while the biofilm layers close to the substratum are dominated by X_3 (Fig. 5.5(A1, A2, A3, A4)). All the substrates $S_j, j = 1, \ldots, 3$ show a fully penetrated profile all over time: S_1 and S_3 are consumed for X_1 metabolism while due to the loss of X_2, S_2 keeps constant after 100 days simulation time (Fig. 5.5(B1, B2, B3, B4)). The heavy metal concentration shows a typical parabolic profile: it decreases going from the bulk liquid to the substratum

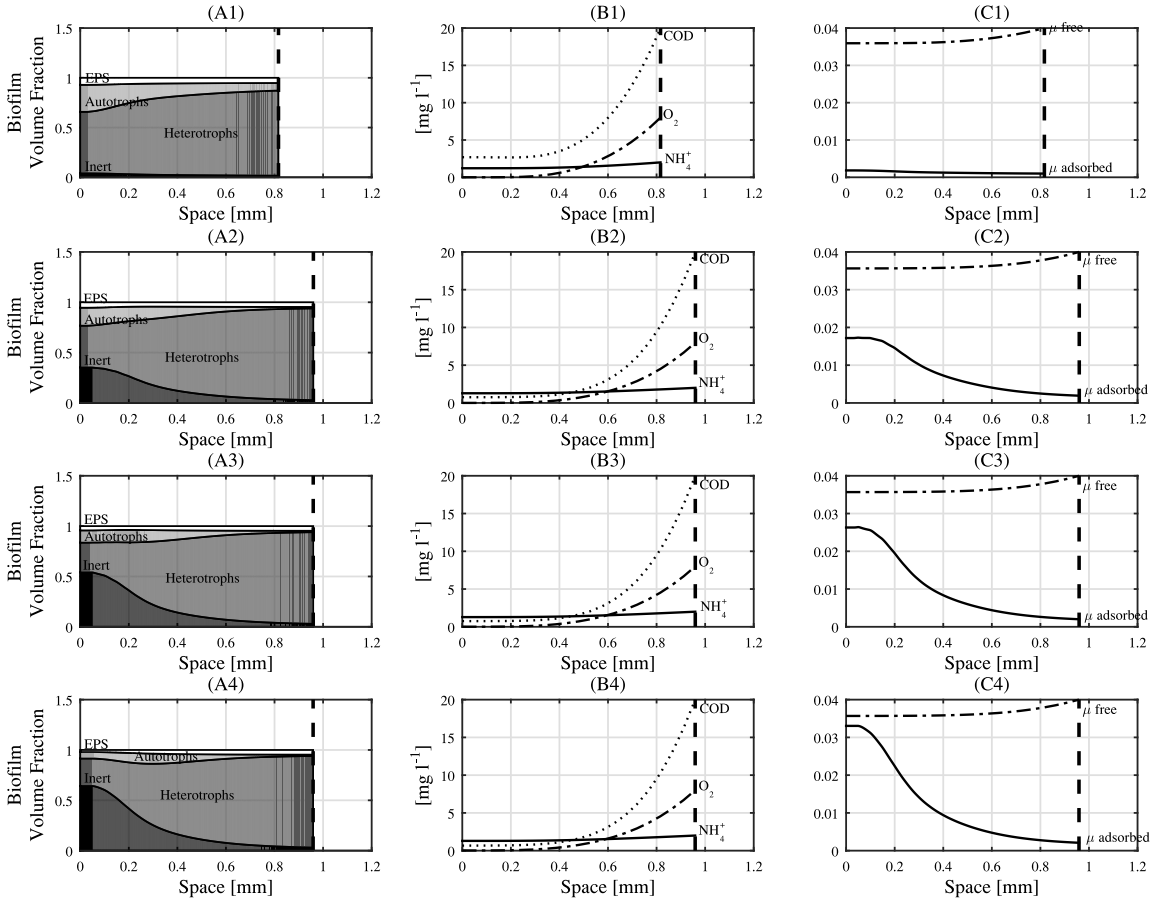

Fig. 5.7. Microbial species distribution (A1, A2, A3, A4), substrate trends (B1, B2, B3, B4), free and adsorbed heavy metal concentrations (C1, C2, C3, C4) after 1, 10, 20 and 100 days simulation time within a heterotrophic–autotrophic biofilm system devoted to wastewater treatment ($k_{ads} = 5, N_1 = 2$). μ_1 concentration is multiplied by a factor of 10^2.

and drops to zero in the middle part of the biofilm as it is consumed by X_1 and progressively adsorbs on it. For what concerns the sorbed heavy metal concentration, it is possible to note that it keeps higher on the free boundary where there is the highest percentage of free binding sites and free heavy metal concentration (Fig. 5.5(C1, C2, C3, C4)). A reduction in biosorption constant leads to a higher microbial diversity and biofilm thickness, a result which is complementary to the previous simulation study confirming model consistency. In Fig. 5.6(A1, A2, A3, A4) it is possible to note that X_2 decreases over time but it is not completely outcompeted by X_1. Indeed, X_2 is able to proliferate in the central/inner part of the biofilm where the formation of an environmental microniche suitable for its growth occurs. This microniche is characterized by the presence in abundance of S_2 and μ_1 while S_1 is close to zero (Fig. 5.6(B1, B2, B3, B4)). As for all the reported simulation sets, the inert represents the most abundant biofilm component in the inner part of the matrix (Fig. 5.6(A1, A2, A3, A4)). S_1 and S_3 are mostly consumed in the outmost part of the biofilm and thus their profiles drop to zero close to the substratum. Conversely, S_2 shows a fully penetrated profile for all the simulation times (Fig. 5.6(B1, B2, B3, B4)). Similarly to S_2, the heavy metal penetrates the whole biofilm and shows a typical parabolic profile: it is consumed by X_1 and X_2 and progressively adsorbs on X_1, accumulating in the form of sorbed heavy metal in the inner part of the biofilm (Fig. 5.6(C1, C2, C3, C4)). A similar result is achieved by further decreasing k_{ads} in simulation *set* 2.3 (Fig. 5.7). The main difference can be observed in Fig. 5.7(C1, C2, C3, C4) in terms of free heavy metal

profile, whose concentration keeps higher all over the biofilm, and sorbed heavy metal which shows a similar trend but in lower concentration than the previous simulation sets.

6. Conclusion

In this work, the qualitative analysis of the free boundary problem related to the biosorption process in multispecies biofilms has been performed. The model takes into account the dynamics of both biofilm components, nutrients and dissolved agents, the latter diffusing from the bulk liquid within the biofilm matrix, where they might participate to the microbial metabolism or be adsorbed on the various biofilm constituents. The dynamics of the sorption sites have been explicitly modeled by considering two systems of nonlinear hyperbolic partial differential equations. An existence and uniqueness result has been proved for the derived free boundary value problem by using the method of characteristics and the fixed point theorem. Numerical simulations related to a real biofilm system dedicated to wastewater treatment and acting as a sorbing agent for heavy metals have been performed. The behavior of the model under different parameter regimes has been analyzed. Simulation results demonstrate the underlying conclusion that biofilm systems can be effectively used in the context of bioremediation and the presented mathematical model can be used as a predictive tool to develop specific treatment plans.

References

[1] H.L. Røder, S.J. Sørensen, M. Burmølle, Studying bacterial multispecies biofilms: Where to start?, Trends Microbiol. 24 (2016) 503–513.
[2] H.C. Flemming, J. Wingender, The biofilm matrix, Nat. Rev. Microbiol. 8 (2010) 623–633.
[3] B.O. Emerenini, B.A. Hense, C. Kuttler, H.J. Eberl, A mathematical model of quorum sensing induced biofilm detachment, PLoS One 10 (2015) e0132385.
[4] G. Robledo, F. Grognard, J.L. Gouzé, Global stability for a model of competition in the chemostat with microbial inputs, Nonlinear Anal. RWA 13 (2) (2012) 582–598.
[5] N.G. Cogan, J.P. Keener, The role of the biofilm matrix in structural development, Math. Med. Biol. 21 (2) (2004) 147–166.
[6] B. Szomolay, I. Klapper, J. Dockery, P.S. Stewart, Adaptive responses to antimicrobial agents in biofilms, Environ. Microbiol. 7 (2005) 1186–1191.
[7] M. Burmølle, D. Ren, T. Bjarnsholt, S.J. Sørensen, Interactions in multispecies biofilms: do they actually matter?, TIM 22 (2) (2014) 84–91.
[8] R. Singh, D. Paul, R.K. Jain, Biofilms: implications in bioremediation, Trends Microbiol. 14 (2006) 389–397.
[9] G.M. Gadd, Biosorption: critical review of scientific rationale, environmental importance and significance for pollution treatment, J. Chem. Technol. Biotechnol. 84 (2009) 13–28.
[10] M. Fomina, G.M. Gadd, Biosorption: current perspectives on concept, definition and application, Bioresour. Technol. 160 (2014) 3–14.
[11] E.R. Rene, K. Pakshirajan, P.N.L. Lens, Special issue on biofilm engineering for heavy-metal removal and recovery, J. Environ. Eng. 142 (2016) C201600.
[12] W.-W. Li, H.-Q. Yu, Insight into the roles of microbial extracellular polymer substances in metal biosorption, Bioresour. Technol. 160 (2014) 15–23.
[13] D. Podstawczyk, A. Dawiec, A. Witek-Krowiak, K. Chojnacka, New trends in microbial biosorption modeling and optimization, in: Handbook of Metal-Microbe Interactions and Bioremediation, CRC Press, 2017, pp. 173–199.
[14] B. D'Acunto, G. Esposito, L. Frunzo, M.R. Mattei, F. Pirozzi, Mathematical modeling of heavy metal biosorption in multispecies biofilms, J. Environ. Eng. 142 (2016) C4015020.
[15] S. Papirio, L. Frunzo, M. Mattei, A. Ferraro, M. Race, B. D'Acunto, F. Pirozzi, G. Esposito, Heavy metal removal from wastewaters by biosorption: mechanisms and modeling, in: Sustainable Heavy Metal Remediation 1: Principles and Processes, Springer, 2017, DOI: http://dx.doi.org/10.1007/978-3-319-58622-9_2 (in press).
[16] D. Kumar, L.K. Pandey, J. Gaur, Metal sorption by algal biomass: From batch to continuous system, Algal Res. 18 (2016) 95–109.
[17] B. Volesky, Detoxification of metal-bearing effluents: biosorption for the next century, Hydrometallurgy 59 (2) (2001) 203–216.
[18] O. Wanner, W. Gujer, A multispecies biofilm model, Biotechnol. Bioeng. 28 (1986) 314–328.
[19] E. Alpkvist, I. Klapper, A multidimensional Multispecies continuum model for heterogeneous biofilm development, Bull. Math. Biol. 69 (2007) 765–789.
[20] B. D'Acunto, L. Frunzo, Qualitative analysis and simulations of a free boundary problem for mulispecies biofilm models, Math. Comput. Modelling 53 (2011) 1596–1606.

[21] L. Frunzo, Modeling sorption of emerging contaminants in biofilms, Federico II Open Arch. (2017). www.fedoa.unina.it/11206/.
[22] F.G. Fermoso, E.D. Van Hullebusch, G. Guibaud, G. Collins, B.H. Svensson, C. Carliell-Marquet, J.P.M. Vink, G. Esposito, L. Frunzo, Fate of trace metals in anaerobic digestion, in: Biogas Science and Technology, Springer, 2015, pp. 171–195.
[23] B.V. Merkey, D.L. Chopp, The performance of a microbial fuel cell depends strongly on anode geometry: a multidimensional modeling study, Bull. Math. Biol. 74 (2012) 834–857.
[24] B. D'Acunto, L. Frunzo, I. Klapper, M.R. Mattei, Modeling multispecies biofilms including new bacterial species invasion, Math. Biosci. 259 (2015) 20–26.
[25] M.R. Mattei, B. D'Acunto, G. Esposito, L. Frunzo, F. Pirozzi, Mathematical modeling of competition and coexistence of sulfate-reducing bacteria, acetogens, and methanogens in multispecies biofilms, Desalin. Water Treat. 55 (2015) 740–748.
[26] M.R. Mattei, L. Frunzo, B. D'Acunto, G. Esposito, F. Pirozzi, Modelling microbial population dynamics in multispecies biofilms including Anammox bacteria, Ecol. Model. 304 (2015) 44–58.
[27] B.V. Merkey, B.E. Rittmann, D.L. Chopp, Modeling how soluble microbial products (SMP) support heterotrophic bacteria in autotroph-based biofilms, J. Theoret. Biol. 259 (4) (2009) 670–683.